Synthesis, Structure, and Bonding of Hypoelectronic $SrIn_4$: Direct Example of a Dominant Size Effect in Structure Selection

Dong-Kyun Seo and John D. Corbett*

Contribution from the Ames Laboratory−DOE[1] and Department of Chemistry, Iowa State University, Ames, Iowa 50011

Received May 30, 2000

Abstract: The structure of the new title compound, the same type as $EuIn_4$, was refined in the monoclinic space group $C2/m$, with $Z = 4$. The compound exhibits a complex three-dimensional network built of four- and five-bonded indium atoms in fused and interbonded pentagons that sandwich the strontium atoms. Both electronic band-structure calculations and property measurements show that the compound is metallic. A detailed band-structure analysis indicates that the compound is hypoelectronic with a one-electron deficiency, but the In−In bonding is effectively optimized in the structure. The important role of cation size in the structure choice is noted in a comparative study of $BaIn_4$, which has the closely related $BaAl_4$-type structure in which barium atoms are sandwiched by six-membered rings.

Introduction

The triels Ga, In, and Tl are remarkable in the compounds that they form with the active metals because they lie to the left of Zintl boundary. These trielide compounds have thus been of great interest for last few decades because their structures exhibit novel clusters and networks that expand our chemistry horizons into the nonclassical valence regime.[2−4] Intrinsic to the trielides are greater degrees of interbonding and condensation. Exploratory synthesis efforts within alkali-metal−triel systems, for indium and thallium especially, have revealed many novel and unanticipated features about their chemistries, not just new classical species, structures, and stoichiometries, but also the presence of evidently the first hypoelectronic clusters relative to Wade's classical rules. The importance of the countercations has been emphasized as well from the synthetic viewpoint; the phase stability has to be eventually achieved in consideration of Madelung energies between cations and anionic clusters, and the structures appear to maximize this effect by filling space efficiently. This is confirmed by the surprising existence of so-called "metallic Zintl phases" in which the cluster anions fulfill the simple electronic requirements for their bonding even in the presence of "excess" free electrons.[2,4] The significant ionic part of the stability can be easily understood by the fact that the triel elements do not exhibit strong covalency in their elemental structures, especially in the case of aluminum (fcc), indium (body-centered tetragonal), and thallium (hcp),[5] whereas gallium, with the smallest atomic size in the group after boron, shows a complicated network.[5,6]

Clearly the Madelung part of phase stability must also be very important in forming structures of three-dimensional networks. Contrary to phases with isolated clusters, the cations must be now encapsulated in sites within the networks, which brings an additional parameter in structure formation, that is, a size match. These aspects are complex in three-dimensional networks and have not been well-explored or generalized. The problems of filling space in an efficient way in a three-dimensionally bonded network are more complex than with isolated clusters, and valence closure in some instances may be only approximately achieved.[2] The scarcely explored alkaline-earth-metal−triel (or rare-earth-metal−triel) systems look particularly suitable to refine these questions and eventually to provide guidelines of understanding. One advantage is that the divalent (or trivalent) cations should afford a larger ionic component to the phase stability. In addition, the electroneutrality in the phases can be achieved by one-half (or one-third) the number of cations that are needed with alkali-metal ions, and hence, three-dimensional networks may form more easily and frequently with the predominant triel atoms.

Tetragonal $BaAl_4$-type compounds remain the exceptional cases in the alkaline-earth-metal−triel systems that have been fully studied, while some other structure types are derived from this prototype.[7,8] The $BaAl_4$-type family of the compounds include $SrAl_4$, $EuAl_4$, $BaAl_4$, $SrGa_4$, $EuGa_4$, $BaGa_4$, and $BaIn_4$.[9] This non-Zintl-type structure effectively optimizes chemical bonding through multi-center electron-deficient bonds as well as two-center two-electron bonding. A monoclinically distorted structure is found for $CaAl_4$[10], $CaGa_4$[11], and $YbGa_4$[12], and the origin of this distortion has been explained.[13] A decade ago, a

(1) This research was supported by the Office of the Basis Energy Sciences, Materials Science Division, U. S. Department of Energy. The Ames Laboratory is operated for the DOE by Iowa State University under Contract no. W-7405-Eng-82.

(2) Corbett, J. D. *Angew. Chem., Int. Ed. Engl.* **2000**, *112*, 682.
(3) Kauzlarich, S. M., Ed. *Chemistry, Structure and Bonding in Zintl Phases and Ions*; VCH: New York, 1996.
(4) Nesper, R. *Angew. Chem., Int. Ed. Engl.* **1991**, *30*, 789.
(5) Donohue, J. *The Structures of the Elements*; Wiley: New York, 1974.
(6) von Schering, H. G.; Nesper, R. *Acta Chem. Scand.* **1991**, *45*, 870.
(7) Zheng, C.; Hoffmann, R. *Z. Naturforsch., B: Chem. Sci.* **1986**, *41*, 292.
(8) Burdett, J. K.; Miller, G. J. *Chem. Mater.* **1990**, *2*, 12.
(9) Villars, P.; Calvert, L. D. *Pearson's Handbook of Crystallographic Data for Intermetallic Phases*, 2nd ed.; Americal Society of Metals: Metals Park, OH, 1991.
(10) Zogg, H.; Schwellinger, P. *J. Mater. Science (London)* **1979**, *14*, 1923.
(11) Bruzzone, G.; Fornasini, M. L.; Merlo, F. *J. Less-Common Met.* **1989**, *154*, 67.
(12) Fornasini, M. L.; Ciafici, S. *J. Less-Common Met.* **1990**, *163*, 331.
(13) Miller, G. J.; Li, F.; Franzen, H. F. *J. Am. Chem. Soc.* **1993**, *115*, 3739.

10.1021/ja001886+ CCC: $19.00
Published on Web 09/22/2000

different monoclinic 1:4 structure was reported in the Eu−In system, but the characterization was far from complete.[14]

During our recently initiated explorations of alkaline-earth-metal−triel systems, a new-phase $SrIn_4$, isostructural with $EuIn_4$, was discovered. Subsequent analysis revealed that the compound, or the structure type, beautifully demonstrates the importance of the alkaline-earth-metal−triel systems in studying the nature of network compounds. In this work, we report its synthesis, structure, chemical bonding characteristics, and relationship to the $BaAl_4$-type structure. The factors governing the structure formation are discussed.

Experimental Section

Synthesis. All reactions were carried out in welded tantalum tubes jacketed in a fused silica container by methods and techniques described previously.[15,16] All materials were handled in N_2- or He-filled gloveboxes that had moisture levels below 0.1 ppm (volume). The title compound was first obtained in an attempt to prepare a ternary phase in the Sr−Ni−In system by utilizing a Sr−In reactive flux. A mixture of strontium, nickel, and indium elements with an atomic ratio of 4.9:1.9:93.2 was heated to 1000 °C, held for 5 h, subsequently cooled at 30 °C/h to 500 °C, then held for 5 days, and finally cooled to room temperature at 7 °C/h. The sample contained single crystals of two phases which could be distinguished by their morphology and sensitivity to air. One compound was readily decomposed in air, probably into SrO and indium metal, but the other was stable in air. A single-crystal X-ray diffraction study showed that the air-sensitive phase was the new $SrIn_4$. The X-ray powder pattern of the other matched well with that calculated for $NiIn_2$.[9]

After the structure of $SrIn_4$ had been established, stoichiometric amounts of elements strontium (Alfa, 99.9%), and indium (Alfa, 99.9995%) were heated to 1000 °C, held for 5 h, quenched, then annealed at 200 °C over a 3-week period and radiatively cooled to room temperature. On the basis of Guinier X-ray powder diffraction, the product was the pure phase. Annealing at 250 °C for 4 weeks gave the same results. An EDX analysis was in agreement with the stoichiometric composition of the samples. A small amount of tantalum (<0.5 at. %) was found by EDX analysis on a rare occasion, and it is attributed to surface contamination from reaction with the Ta vessels.

Experiments under dynamic vacuum were carried out to ascertain that no hydride impurities were present. To rule out possible existence of hydrogen in the starting materials, 400−600 mg of strontium metal was sealed in a welded Ta container, which was in turn encapsulated in a fused silica tube connected to a high vacuum system, heated to 900 °C, held for 12 h in a dynamic vacuum, and cooled to room-temperature radiatively. The strontium exhibited a brighter luster after the treatment. The high vacuum system was equipped with a mercury diffusion pump, and routine work with this system gave a vacuum below discharge of a Tesla coil, that is, $\sim 10^{-5}$ Torr. A cold trap cooled with liquid N_2 was kept between the line and the silica tube. This purified metal produced no changes in the $SrIn_4$ syntheses. Some Sr−In reactions under dynamic vacuum were also done in the same way as in sealed jackets under static vacuum, but with 2 days of annealing at 500 °C. The XRD powder pattern of the reaction product showed the $SrIn_4$ phase in high yield (>∼80%).

Structure Determination. Shiny, silvery block-shaped crystals were picked up in the glovebox and sealed in thin-walled capillaries, and Laue photographs were used to determine which crystal was most suitable for structural determination. Diffraction data were collected at 23 °C on a Rigaku AFC6R automatic diffractometer with monochromated Mo Kα radiation. Cell constants and an orientation matrix for data collection were determined from a least-squares refinement of the setting angles of 25 centered reflections. In total, 1702 reflections were measured for the C-centered monoclinic cell in the four octants $h, \pm k, \pm l$ up to $2\Theta = 60°$; of these, 1008 reflections were observed [$I/\sigma(I) > 3$]. Intensity statistics indicated a centrosymmetric space group ($\langle E^2 - 1 \rangle = 0.913$), and the refinement proceeded successfully in $C2/m$. The diffraction data were corrected empirically for Lorentz polarization effects and for absorption with the aid of three ψ-scans. Some details of the data collection and refinement are listed in Table 1. The structure was solved by direct methods utilizing the program package SHELXTL.[17] Secondary extinction was taken into account during the refinement. The full-matrix least-squares refinement converged at $R(F) = 3.4\%$, wR2 = 6.1%, and GOF = 1.000 for 31 variables and 900 independent reflections. The maximum and minimum peaks in the final difference Fourier map were 1.63 (0.68 Å from In1) and -1.47 e$^-$/Å^3. The only faint indication of any problem might be a slight asymmetry of the anisotropic displacement ellipsoids observed for In2 and In4 (U_{11}:U_{22}:$U_{33} \approx$ 2.7:1.7:1 and 2.1:1.8:1, respectively). As will be seen, these atoms have the two longest In−In bonds in the structure (3.324, 3.279 Å). The slight elongation of their anisotropic ellipsoids, parallel to the long bond direction, is not a likely indication of any crystallography error. Similarly, the reported isotropic thermal parameters of $EuIn_4$ also have larger values for In2 and In4.[14]

Table 1. Selected Data Collection and Refinement Parameters for $SrIn_4$

space group, Z	$C2/m$ (no. 12), 4
fw	1093.80
lattice parameters (Å, deg)[a]	$a = 12.079(3)$
	$b = 5.1245(17)$
	$c = 9.920(3)$
	$\beta = 114.85(2)$
volume (Å^3)	557.2(3)
r_{calcd} (gcm^{-3})	6.519
μ (Mo Kα, cm^{-1})	256.41
$R1$, wR2[b]	0.034, 0.061

[a] Data from Guinier powder pattern; $\lambda = 1.540\,562$ Å. [b] $R1 = \Sigma||F_o| - |F_c||/\Sigma F_o|$, $wR2 = \{\Sigma[w(F_o^2 - F_c^2)^2]/\Sigma[w(F_o^2)^2]\}^{1/2}$.

Table 2. Atomic Coordinates (× 10^4 Å) and Isotropic-Equivalent Thermal Parameters for (× 10^3 Å^2) for $SrIn_4$

	x	y	z	B_{eq}[a]
Sr	1649(1)	0	7089(1)	19(1)
In1	1551(1)	0	3506(1)	21(1)
In2	1501(1)	0	532(1)	32(1)
In3	4244(1)	0	5782(1)	18(1)
In4	4357(1)	0	1007(1)	29(1)

[a] B_{eq} is defined as one-third of the trace of the orthogonalized $\mathbf{U}_{ij}$ tensor.

Table 2 gives the atomic positional and isotropic-equivalent thermal parameters, and Table 3 lists important interatomic distances in the structure. Additional crystallographic data and the anisotropic displacement parameters are given in the Supporting Information, and the F_o/F_c listings and other information are available from J.D.C.

Properties. Electrical resistivity was measured at 35 MHz over 110−300 K by the electrodeless "Q" method with the aid of a Hewlett-Packard 4342A Q Meter.[18] For this purpose, 66.9 mg of a powdered sample with grain diameters between 150 and 250 μm was dispersed with chromatographic alumina and sealed under He in a Pyrex tube. The measured specific resistivities increased from about 16 to 22 $\mu\Omega\cdot$cm over the range of 100−260 K (0.2% K^{-1}). Magnetic susceptibility measurements made over 6−300 K on a Quantum Design (MPMS) SQUID magnetometer on two separate, single-phase samples. Each of the powdered samples was held between two fused silica rods that were in turn fixed and sealed inside a silica tube. The data were corrected for the container and the standard diamagnetic core contributions.

EHTB Calculations. All of the calculations were carried out using the CAESAR program.[19] A weighted H_{ij} formula was used for the extended Hückel calculations, and the following atomic orbital energies and exponents were employed for all of the calculations (H_{ij} = orbital

(14) Fornasini, M. L.; Ciafici, S. *Z. Kristallogr.* **1990**, *190*, 295.
(15) Corbett, J. D. *Inorg. Synth.* **1983**, *22*, 15.
(16) Corbett, J. D. In *Solid State Chemistry − Techniques*; Cheetham, A. K., Day, P., Eds.; Clarendon Press: Oxford, England, 1987; Chapter 1.
(17) SHELXTL; Bruker AXS, Inc.: Madison, WI, 1997.
(18) Zhao, J.-T.; Corbett, J. D. *Inorg. Chem.* **1995**, *34*, 378.
(19) Ren, J.; Liang, W.; Whangbo, M.-H. *CAESAR for Windows*; Prime-Color Software, Inc., North Carolina State University: Raleigh, NC, 1998.

Table 3. Selected Bond Distances in $SrIn_4$ (D)

In1−In2[a]	2.926(1)	In4−In3[a]	2.912(2)
In1−In3	2.926(1) × 2	In4−In2	2.939(1) × 2
In1−In3[a]	3.083(2)	In4−In4[a]	3.003(2)
In1−Sr[a]	3.506(2)	In4−In2[a]	3.279(2)
In1−Sr	3.566(1) × 2	In4−Sr	3.680(1) × 2
In1−Sr[a]	3.658(2)		
		Sr−In2	3.495(2)
In2−In1[a]	2.926(1)	Sr−In1	3.506(2)
In2−In4	2.939(1) × 2	Sr−In2	3.563(1) × 2
In2−In4[a]	3.279(2)	Sr−In1	3.566(1) × 2
In2−In2[a]	3.324(2)	Sr−In3	3.641(1) × 2
In2−Sr[a]	3.495(2)	Sr−In1	3.658(2)
In2−Sr	3.563(1) × 2		
		Sr−In3	3.677(1) × 2
In3−In3[a]	2.850(2)	Sr−In4	3.680(1) × 2
In3−In4[a]	2.912(2)	Sr−In3	3.863(2)
In3−In1	2.926(1) × 2	Sr−In4	3.889(2)
In3−In1[a]	3.083(2)	Sr−Sr	4.378(3)
In3−Sr	3.641(1) × 2	Sr−Sr	5.125(2) × 2
In3−Sr	3.677(1) × 2		

[a] Bond distances in the planes at $y = 0,1/2$.

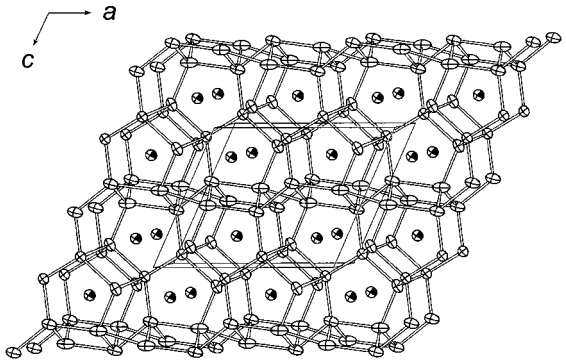

Figure 1. Off-[010] section of the monoclinic unit cell of $SrIn_4$ down the short *b* axis; 90% ellipsoids. All atoms lie in the same type of mirror planes at $y = 0$ or 1/2, and these planes of atoms repeat along *b* displaced by *a*/2 owing to a *C*-centering. Pentagon dimers at $y = 1/2$ are centered about 0,0. Indium atoms are crossed, and strontium atoms quarter-shaded.

energy, ζ = Slater exponent): In 5s, $H_{ii} = -12.6$ eV, $\zeta = 1.903$; 5p, −6.19 eV, 1.677;[20] Sr 5s, −6.62 eV, 1.214; 5p, −3.92 eV, 1.214.[21]

Results and Discussion

Structural Description. The structure of $SrIn_4$ can be described as a three-dimensional fused-cluster network of indium atoms in which strontium atoms are encapsulated, one per cage. The general [010] view of the unit cell in Figure 1 has all In−In distances less than 3.4 Å outlined. There is only one type of cage, of a rather unsymmetric shape, defined by indium atoms. Each cage has two pentagonal rings perpendicular to the view direction $\vec{b}$ that sandwich a strontium atom (see, for example, the anionic environment of the third strontium atom from the left at the top in Figure 1). These two rings are held together along $\vec{b}$ by five indium atoms in an intervening layer in the *ac* plane that are actually parts of other pentagonal rings. Of these five, four are bonded together in pairs (parts of other pentagonal rings, Figure 2), and then those pairs are connected through an indium that is also one of the paired atoms in the neighborhood.

A different and detailed view of the indium network in $SrIn_4$ is more beneficial, as will be seen soon. Figure 2 is depicted to differentiate In−In bonds that lie *in* and *between* the mirror

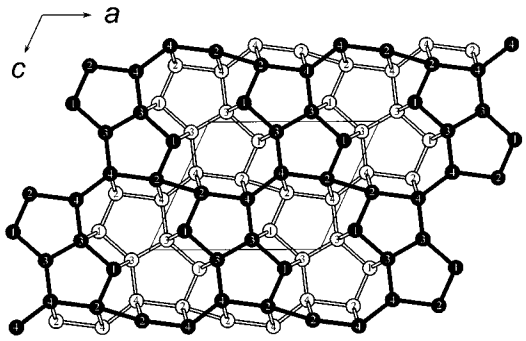

Figure 2. Projection of the indium network in the structure of $SrIn_4$ down the short axis *b*. Indium atoms at $y = 1$ are presented in solid circles, and those at $y = 1/2$ in open circles. Edge-sharing pentagon dimers are centered at 1/2,1,0 (solid), and 0,1/2,0 (open). All strontium atoms lie midway between these pentagon dimeric units.

planes in the structure (called *in-plane* and *interplane* bonds, hereafter). All atoms lie in a single type of plane at $y = 0$ or 1/2 that has two positions because of the displacement of $(\vec{a} + \vec{b})/2$ from the *C*-centering operation. The building unit in each plane is an edge-sharing pentagon dimer. The four atoms on the outer edges of each dimer are connected to the neighboring dimers to define large, intervening 12-membered rings. The 2-fold symmetry elements of the space group along $\vec{b}$ (at 0,0 and 1/2,0, etc) are well-reflected in the shapes of both the pentagon dimers and the 12-membered rings. A nearly linear tetrameric unit (In4−In2−In2−In4) is noted along $\vec{a}$, with In2−In2−In4 angles of 171°. This fragment has the longest In−In bonds in the indium network ($d_{In2-In2} = 3.324$ Å; $d_{In2-In4} = 3.279$ Å). In comparison, the other In−In bond distances are 2.91−3.08 Å. The same is true in $EuIn_4$ for which the corresponding longest In−In bond distances are 3.395 and 3.203 Å.[14]

An emphasis on the connectivity between these planes leads to the recognition of two different types of double zigzag chains that run along $\vec{b}$; one made of −(In2−In4−In2−In4)− zigzag units, and the other, of −(In1−In3−In1−In3)− units. Therefore, the indium network can be alternatively considered to be built by perpendicular bond formations in the *ac* plane that interconnect those two types of double zigzag chains. In fact, a variety of solid-state frameworks have double zigzag chains as their structural motif. Mesoscopic tunnels in the zeolites-like cancrinite and MAPO-36 and -39 are formed and surrounded by double zigzag chains running parallel to each other.[22] Closer examples include $BaIn_2$[23] ($CeCu_2$- or $SrAl_2$-type), Sr_3In_5[24] (Ca_3Ga_5-type[25]), and $BaIn_4$[26] ($BaAl_4$-type). In the former two compounds, the indium double zigzag chains are connected together either through direct bonding or via intermediate indium atoms. All atoms in the chains have single bonds to the neighboring four atoms. In tetragonal $BaIn_4$, Figure 3, the double zigzag chains along $\vec{a}$ (and $\vec{b}$) are completely fused together side to side to form waggled layers lying perpendicular to $\vec{c}$. The three-dimensional network is then constructed by bond formation between the outer atoms of the neighboring layers. One barium atom is sandwiched between two hexagons separated by a unit cell distance. In the same manner previously applied for $SrIn_4$, the network in $BaIn_4$ can be described as the

(20) Canadell, E.; Eisenstein, O.; Rubio, J. *Organometallics* **1984**, *3*, 759.
(21) Hinze, J.; Jaffé, H. H. *J. Chem. Phys.* **1963**, *67*, 1501.
(22) O'Keeffe, M.; Hyde, B. G. *Crystal Structures − I. Patterns and Symmetry*; Mineralogical Society of America: Washington D. C., 1996; p 307.
(23) Bruzzone, G. *Atti Accad. Naz. Lincei* **1970**, *48*, 235.
(24) Seo, D.-K.; Corbett, J. D. To be submitted.
(25) Cordier, G.; Schäfer, H.; Stelter, M. *Z. Anorg. Allg. Chem.* **1986**, *539*, 33.

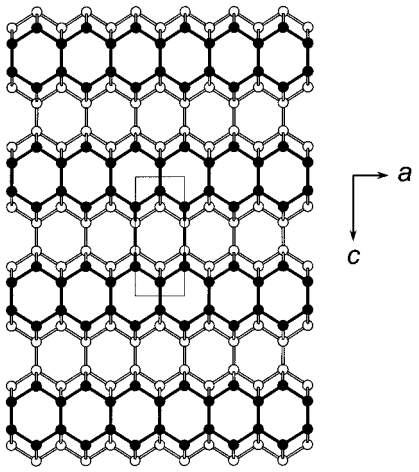

Figure 3. Projection of the indium network in the tetragonal structure of $BaIn_4$ down a short axis *b*. All atoms lie in the same type of planes at $y = 0$ or 1/2 but repeat along *b* displaced by *c*/2 because of a glide plane. Indium atoms at $y = 1/2$ are presented as open circles and those $y = 1$, with solid circles.

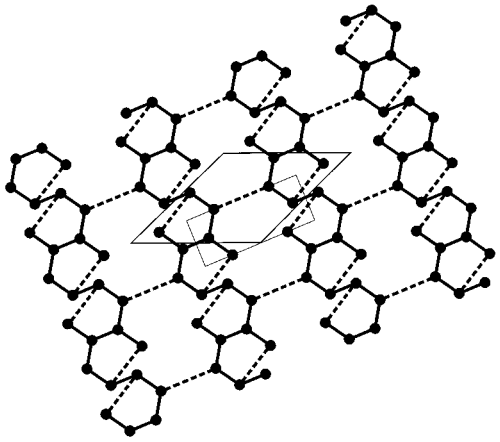

Figure 4. Top indium layer (solid circles and lines) in Figure 3 is redrawn here, tilted by ~67°. Hexagons are transformed by bond breaking and formation within the hexagons. Broken lines indicate newly formed bonds. Additional bond formation between the hexagon chains is also noted. The new oblique unit cell has a doubled volume and is depicted with the thicker cell boundaries.

flat layers interconnected through the interplane bonds, the layers being composed of isolated parallel chains of edge-sharing hexagons in the *bc* (or *ac*) plane, as seen in Figure 3. The In−In bond distances in all three indium compounds range from 2.81 to 3.10 Å.

In particular, $BaIn_4$ is interesting because it has the same composition as $SrIn_4$, but at first glance it exhibits a strikingly different structure. Although a real structural change or transition is not claimed, a good relationship between the two structural types can be deduced by a closer examination as follows. In Figure 4, the top layer with solid circles and lines from Figure 3 is drawn again, but now tilted so that a rhombic unit cell with doubled volume is oriented to have a horizontal axis in the picture. Each hexagon is transformed into a (distorted) pentagon by breaking one outer bond and then by forming a new bond between the outer and inner atoms on the opposite side of the chain in such a way that the newly formed pentagons share their edges in pairs and retain the 2-fold symmetry elements. The other outer atoms that are not involved in this process are connected to those in the neighboring chain. The result is a layer with the topological connectivity of the indium layer in $SrIn_4$ (Figure 2). The rhombus in Figure 4 corresponds

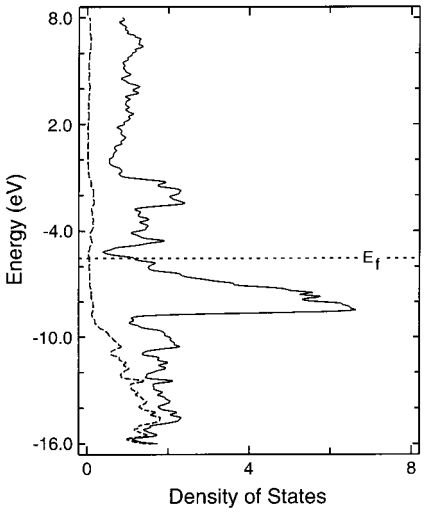

Figure 5. DOS plots calculated for the In_4^{2-} anionic sublattice of $SrIn_4$. Solid and dashed lines refer to the total DOS and the projected DOS of 5s orbitals, respectively. The calculation was carried out on the primitive unit cell with two formula units.

to the base of the monoclinic unit cell of $SrIn_4$. The collapse of the hexagons into pentagons, as well as the interchain bond formation, indicates that the structural deformation leads to smaller pockets for the accommodation of smaller cations. This is in agreement with the fact that the strontium is smaller than barium. Further implications are presented in a later section.

Electronic Structure. The structure of $SrIn_4$ (and $BaIn_4$) clearly cannot be understood from the simple Zintl rule, that is, with octet formulations. In $BaIn_4$, two five-bonded indium atoms essentially have three-center two-electron bonds with two neighboring four-bonded indium atoms, although they form two-center two-electron bonds between themselves. The necessary decrease in hole size in $SrIn_4$ leads to three five-bonded indium atoms and one that is four-bonded, In1. The much more complicated catenation pattern of the indium network in $SrIn_4$, combined with lower local symmetries around individual indium atoms, does not permit any simple electron count formulation for the network without the help of electronic structure calculations.

The electronic band structure was calculated for both the indium sublattice and the complete structure of $SrIn_4$. The densities-of-states (DOS) and crystal orbital overlap populations (COOP) from the former are plotted in Figures 5 and 6, respectively, where the 14 valence electrons per In_4 fill the orbitals up to a Fermi energy of −5.54 eV. The calculation indicates a metallic behavior for the compound. Judging from the COOP curve, a sharp DOS peak found right below the Fermi energy has a strong bonding character. The s orbital contribution to the DOS, Figure 5, is highly concentrated below the large valence-based peak, indicating that s−p mixing is not large. The unfilled energy region of −5 to −1 eV contains a relatively large number of states. However, the bonding character changes gradually from bonding to antibonding in this region (Figure 6), and orbital interactions are weak because the magnitudes of COOP are small. Inclusion of strontium atoms in the calculations provides essentially the same picture. The main difference is that the weakly bonding region above −5 eV for the anion lattice is now slightly raised by ~0.4 eV, with the largest COOP value of ~0.03. However, this small gain of In−In bonding character is compensated by a larger antibonding character (the lowest COOP = ~−0.04) from Sr−In interactions in the same energy region.

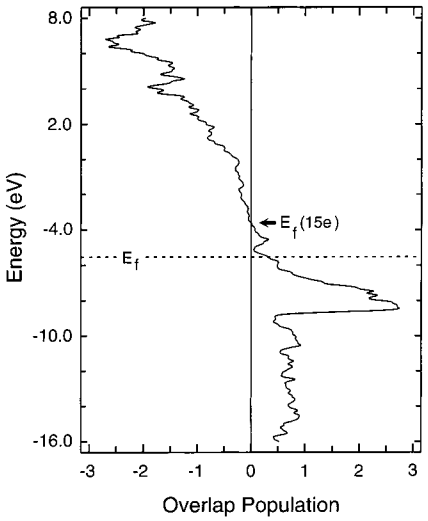

Figure 6. COOP curve calculated for all of the In−In distances within 3.5 Å for the In_4^{2-} sublattice. Calculation was carried out on a primitive unit cell with two formula units. Arrow indicates the hypothetical Fermi energy that would correspond to 15 valence electrons per formula unit; i.e., In_4^{3-} (see text).

To fill all of the bonding levels in Figures 5 and 6, one additional electron would be needed per In_4; that is, the optimum number of valence electrons is 15 per In_4. Therefore, the compound is still hypoelectronic in this structure, having a one-electron deficiency (or two electrons to give a classical four-bonded structure). Interestingly, however, this electron deficiency does not seem to mean that $BaAl_4$-structure type is preferred in terms of electronic effects. The calculated total electronic energy of the In_4^{2-} lattice in $SrIn_4$ is −150.1 eV per In_4, which is only slightly higher than the −150.4 eV calculated for the same 14 e^- in the In_4^{2-} lattice of $BaIn_4$. It should be remembered that the catenation pattern and the bonding scheme of the indium lattice in $BaIn_4$ does not follow Zintl rules, either. However, it is plausible to assume that a hypothetical strontium analogue of $BaIn_4$ would have a significantly lower anionic sublattice energy because the In−In distances would be shorter in this version than in $BaIn_4$. This is true at least between $SrAl_4$ and $BaAl_4$ having the same structure type.[27] In any case, the $SrIn_4$ structure is clearly the more stable in total enengy, and this originates with the smaller cation.

The band structure of the indium network of $SrIn_4$ can be qualitatively understood by recognizing that the p orbitals in interplane and in-plane bonds are rather separable and behave more-or-less independently. Consider the zigzag chains (along $\vec{b}$) first, Figure 2. These have bond angles of 121∼122°, and each indium atom in the network is a part of a zigzag chain. Such chains have been well-studied in the literature.[28] Two interplane bonds are formed per indium site along the chain direction, and these appear as two broad bands with a band gap in the band structure, one bonding and the other nonbonding. The orbital mixing gives rise to a nonbonding orbital in the plane of the chain. Because s−p mixing is found to be weak in the indium network (Figure 5), the nonbonding orbital can be approximated as a p orbital. This orbital, as well as another π-type p orbital in the chains, weakly interacts along the chain direction. They are located in energy between the bonding and antibonding bands of the interplane bonds and are expected to be heavily involved in bond formation within the layers, that is, perpendicular to the chain direction. On the contrary, the character of the two-center two-electron bonds formed along the chains may not be perturbed greatly by the in-plane interactions. Thus, we now turn our attention to the interactions between the in-plane orbitals, which are more complicated because of the complexity of the layers shown in Figure 2.

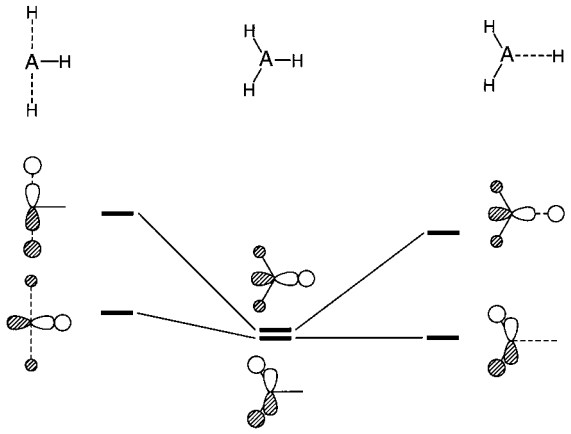

Figure 7. Schematic diagram showing the energy changes of two in-plane MOs according to the two different types of distortions from a regular triangular geometry of a hypothetical AH_3. From left to right, the columns correspond to the idealized local geometries around In2, In3, and In4, respectively. Longer bonds are denoted with broken lines. The s−p mixing is assumed to be negligible.

Figure 7 presents idealized bonding molecular orbitals (BMOs) from the in-plane p orbitals for three cases of indium atoms bonded differently to three hydrogen ligands in the same plane. The columns from left to right represent the local coordinations around In2, In3, and In4; s−p mixing is neglected. While In3 (center) has an in-plane coordination close to a regular triangle, In2 and In4 have two and one longer bonds with indium neighbors, respectively. Further deformation to a T-shape is found in the case of In2. The BMOs of In3 in Figure 7 are degenerate with the same amount of bonding. The bond lengthening in the coordination geometries of In3 and In4 significantly reduces overlap between one of the two indium p orbitals directed toward the lengthened bond and the neighboring orbitals. This is shown in the left and right columns in Figure 7 where one BMO is raised significantly. Although, in fact, things will be much more complicated, one might expect to see this effect in the real extended indium network of $SrIn_4$. For this purpose, we modeled a hypothetical layer of indium that is terminated in the normal direction by hydrogen-like atoms, *X*'s, to replace indium atoms in the adjoining layers. The layer has a oblique unit cell, which is the base of the monoclinic cell of $SrIn_4$ (see Figure 2). There are two asymmetric units made of four indium atoms (In1:In2:In3:In4 = 1:1:1:1) in a unit cell, and hence, 16 in-plane bands are expected. The *X* atoms were generated to imitate indium atoms such that their 1s orbitals were given the p orbital energy of indium. However, the orbital exponent of hydrogen was utilized for *X*, as well as an In−*X* distance (1.85 Å), to avoid the interactions between the terminal atoms.

Figure 8 presents the p-block bands calculated for this hypothetical In_8X_{16} layer. The bands of in-plane character are emphasized with bold lines, and the out-of-plane bands are drawn in thin lines. There are six narrow in-plane bands at low energies, overlapping with out-of-plane bands that exhibit a bonding character. The bottom part of the other six in-plane bands, antibonding with much higher energies, is at the top of

(26) Bruzzone, G. *Acta Crystallogr.* **1965**, *18*, 1081.
(27) Göbel, S.; Somer, M.; Carrillo-Cabrera, W.; Peters, E.-M.; Peters, K.; von Schnering, H. G. *Z. Kristallogr.* **1996**, *211*, 189.
(28) See, for example, Miller G. J. in reference 3, pp 31−37.

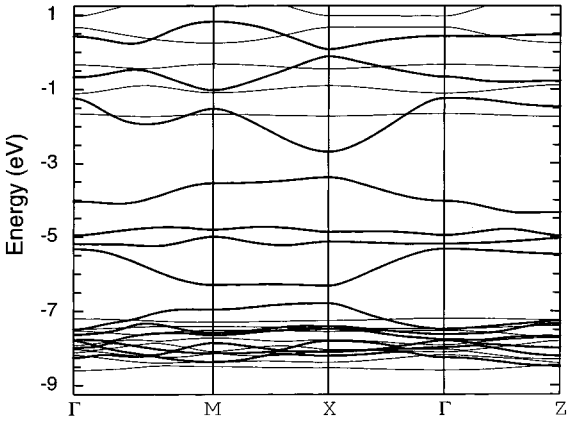

Figure 8. Dispersion relations of the bottom part of the p-block bands of a hypothetical In_8X_{16} layer. Two artificial atoms, *X*, terminate each indium atom vertically (see text). Bold and thin curves exhibit in-plane and out-of-plane character, respectively. $\Gamma = (0,0)$, $M = (\mathbf{a}^*/2,\mathbf{c}^*/2)$, $X = (\mathbf{a}^*/2,0)$, and $Z = (0,\mathbf{c}^*/2)$ where **a**, and **c** are the unit cell vectors of $SrIn_4$.

the dispersion relations. From the comparison of their energies to the atomic orbital energy of indium 5p (−6.19 eV), it can be said that the four middle in-plane bands (−6.7 to −3.2 eV) should have weak orbital interactions, probably composed of In2 and In4. Although not shown here, a crystal orbital analysis proves that these four bands are indeed from a linear In−In2−In2−In4 tetramer with the characteristic long interatomic distances in the layer and, furthermore, they originate especially from four in-plane p orbitals *parallel* to the tetramer. These p orbitals in the lowest band among the four bands are aligned in-phase, thereby resulting in a weak bonding character for the band. The two narrow bands right above are nonbonding. The highest among the four shows additional strong out-of-plane interactions having antibonding character.

In conclusion, the band structure in Figure 8 suggests that there are three strongly bonding bands and three strongly antibonding bands in-plane per In_4. Suppose that these six bands originate from six in-plane p orbitals strongly interacting with neighbors, and that the local symmetry around the individual indium atoms is low enough for strong band repulsion. As seen in Figure 7, In2, In3, and In4 atoms provide a total of four p orbitals of such a kind. The other two are from In1. Meanwhile, the two weakly interacting orbitals from In2 and In4 end up forming two more-or-less nonbonding bands per In_4. Certainly, this simple bonding scheme is a highly approximate one that was devised to focus on the electronic nature of only in-plane orbital interactions. The big discrepancy for this model is that the large band gaps formed between the bands of different bonding characters do not appear in the three-dimensional band structure. Because the interplane bands have to be quite broad in the three-dimensional structure, in fact, the in-plane and interplane bands do overlap and are not completely separable, perturbing our initial assumption of independent in-plane and interplane orbital interactions.

Nonetheless, this simple bonding scheme seems to explain the electron counting for the complicated three-dimensional indium network of $SrIn_4$ quite well. This is just because the zigzagging in the indium double chains, which are perpendicular to the planes, ensures classical two-center two-electron bonds from interplane orbital interactions, and hence, those bonds are still separable from the in-plane bonds as far as the electron counting is concerned. There will be six electrons per In_4 responsible for bond formation in-plane when the strongly bonding bands are filled. Because 2 more electrons per indium

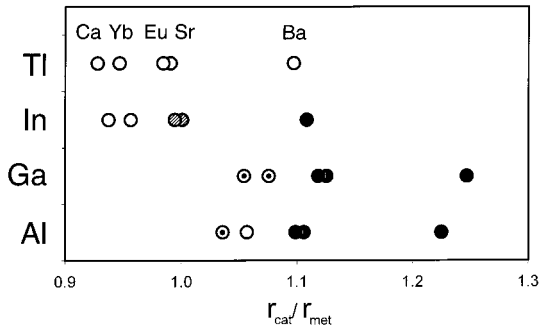

Figure 9. Size ratios of some divalent metals and the group-13 elements. For the active metals, 12-coordinate cation radii are chosen (see text). Radii of the group-13 elements are from their element structures. Typic phases of $BaAl_4$-, $EuIn_4$ ($SrIn_4$)-, and $CaAl_4$-types, are marked with solid, shaded, and centered circles, respectively. Cation order is the same for each period. Open circles indicate that the corresponding 1:4 phase does not exist or has not been identified in their binary systems.

site participate in the inter-plane bonds along the chain direction (8 electrons per In_4), the network needs a total of 14 valence electrons per In_4, that is, 2 extra valence electrons per In_4. This is exactly what happens in $SrIn_4$. We conclude that in $SrIn_4$ all bands with a strong bonding character are completely filled, whereas other weakly bonding and antibonding bands are empty. Were all the bonding bands to be completely filled ($E_f \simeq -5.3$ eV), Figure 8, the compound would be electron-precise with 15 valence electrons per In_4. This is in agreement with what we observed for the three-dimensional band structure in Figure 6. In the extreme situation, the network may hold up to 17 valence electrons per In_4, filling electrons up to the ninth in-plane band in Figure 8. In Figure 6 ($E_f = -4.7$ eV), the corresponding Fermi energy is −1.5 eV, which lies almost at the top of the weakly antibonding energy region. It is noted that the weakly bonding nature near the Fermi level comes from the longer bonds localized in the linear In4−In2−In2−In4 unit. Thus, for a complete electronic structure analysis of the indium network in $SrIn_4$, it is important ultimately to consider actual bond distances, not just topological aspects of the network. This conclusion does not change even for the complete structure calculations with strontium included.

Size Effects. The comparable total electronic energies of indium networks in $SrIn_4$ and $BaIn_4$ imply that the In−In bonding does not preferentially stabilize either of the structure types to a great degree, and the additional Sr−In orbital interactions contribute no significant changes to the electronic energy structures. As alluded to, the size of the cations should be related to the structure formed; the smaller cations prefer the $SrIn_4$-type structure because of its smaller cation cages and the higher Madelung energy, as well. The radii of some divalent cations relative to those of the group-13 elements are plotted in Figure 9. Similar plots are found in the literature for the studies of phase stability of $BaAl_4$-type compounds.[7,29] In our plot, Shannon's ionic radii[30] with a CN 12 are used for the cations, and the radii of the group-13 elements are taken from their elemental structures.[31] The radii of Eu and Yb were deduced from the extrapolation of their radii for the lower coordination numbers, assuming that their behavior follows that of the other cations.

In Figure 9, the $BaAl_4$- and $EuIn_4$-type ($SrIn_4$) compounds appear well-separated in the span of size ratios. The $EuIn_4$-

(29) Bruzzone, G. *Acta Crystallogr.* **1969**, *B25*, 1206.
(30) Shannon, R. D. *Acta Crystallogr.* **1976**, *A32*, 751.
(31) Pauling, L. *The Nature of the Chemical Bond*, 3rd ed.; Cornell University Press: Ithaca, NY, 1960; p 402.

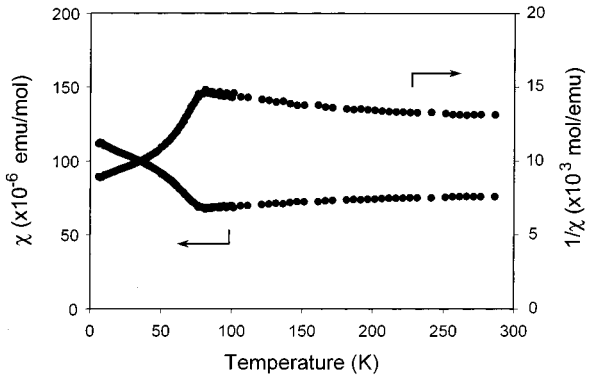

Figure 10. Magnetic susceptibility of $SrIn_4$, measured on heating at 3*T*. Three data sets are plotted below 100 K. Above 83 K, the data indicate a Pauli-paramagnetic compound.

type compounds occur below 1.02, but the $BaAl_4$-type compounds are preferred above 1.08. It is apparent that the $BaAl_4$-type can be stabilized or maintained only by large cations, and not by smaller ones. The opposite is the case for $EuIn_4$-type structure. This exactly mirrors the relationship between CsCl-type and NaCl-type structures. For a given cation, the Madelung energy is generally greater in a NaCl-type structure than in a CsCl-type, because the former is guaranteed to have shorter cation−anion distances whenever the anion spheres are in contact. It is the larger size of the cesium ion that prevents its adoption of a NaCl-type structure, although the restriction is lifted for the sodium ion.

In the narrow region between the two regimes (1.02∼1.08), $CaAl_4$, $CaGa_4$, and $YbGa_4$ occur with a small monoclinic distortion of the $BaAl_4$ structure at room temperature. Especially for $CaAl_4$, a phase transition from tetragonal to monoclinic symmetry has been reported at 140 °C. Although the transition was attributed to an electronic effect in the previous study,[13] a size effect may play a significant role, as well.

Magnetic Susceptibility. Magnetic susceptibility data for $SrIn_4$ are shown in Figure 10 for a single phase sample annealed at 250 °C for 4 weeks. The same results were obtained for an independent sample annealed at a different temperature (200 °C). The compound is essentially Pauli-paramagnetic above ∼83 K, which is in agreement with the expected metallic behavior and the measured resistivities (Experimental Section). A sharp transition occurs around 83 K, and the magnetic susceptibility increases continuously by up to ∼140% as the temperature is decreased to 6 K. The tantalum tubing used as a reaction container does not seem to be a plausible source of such magnetic impurities. There has been no report concerning the formation of tantalum compounds with indium and/or strontium or of the terminal solid solution phases on the indium-rich end. Furthermore, no such signals have ever been found in the many magnetic studies of other analogous indium compounds.[32] The reproducible results indicate that the anomaly is intrinsic. Recent experiments on doped hexaborides, $La_xCa_{1-x}B_6$ ($x = 0.0025-0.1$) and $Ba_{0.005}Ca_{0.995}B_6$, show that the compounds exhibit a weak ferromagnetism, although the DOS at the Fermi level is quite small.[33] Their behavior above the transition temperature (600 K) does not follow the Curie−Weiss law, the same as $SrIn_4$. This weak itinerant ferromagnetism below the Stoner limit has been reproduced in theoretical studies.[34] Interestingly, impurities of the strontium used as our starting material are predominantly calcium and barium,[35] and hence, the actual formula of our $SrIn_4$ should be $(Ca,Ba)_{0.001}Sr_{0.999}In_4$, which resembles the situation of the doped hexaborides. Otherwise, the abnormality can be innate to $SrIn_4$ itself. For conclusive answers, further investigations of the magnetic properties of $SrIn_4$ in a collaboration are in progress, although our preliminary results with our original samples show ferromagnetism.

(32) For example, see Corbett, J. D. in ref. 3, p 172.

Conclusion

The newly discovered metallic compound $SrIn_4$ exhibits the $EuIn_4$-type structure which has a much more complicated indium network than that of $BaIn_4$, a member of the famous $BaAl_4$ family. Extended-Hückel electronic band structure calculations suggest that the electronic energy of the indium networks in $SrIn_4$ is comparable to, or very slightly higher (less stable) than, that of $BaIn_4$. The structure selections very likely depend strongly on the relative sizes of the alkaline earth element and the cavities presented by the group-13 elements in each. This is understandable from the structural correlations between the two structure types; that is, the indium network of $SrIn_4$ ($EuIn_4$-type) is formed from that of $BaAl_4$ by the collapse of surrounding triel hexagons into pentagons plus an interconnection between opposite indium atoms in the cation cages. The resultant lower symmetry structure is much more complicated and contains more In−In bonds. However, the band structure analysis shows that the In−In bonding in the network of $SrIn_4$ is effectively optimized, with all of the valence electrons in strongly bonding bands. This is achieved by lengthening bonds in the linear part within layers of the structure, and hence, through creation of weakly bonding bands that are left empty. In conclusion, this work directly illustrates the importance of cation size in structure selection, as well as a clever structural adaptation for the given cations (size, number, and charge).

The success of the electronic theories has been impressive in the rationalization of different types of structure formation and the stabilities of a diverse range of materials, from classical Zintl compounds to Wade clusters to Hume−Rothery phases. The overwhelming number of successful treatments actually has left us biased toward electronic effects in the consideration of the structures of and the bonding in these materials. This study clearly demonstrates that the electronic factors are not the only ones to look for in studying the structures of intermetallics positioned beyond the Zintl boundary.

Supporting Information Available: Tables of additional crystallographic data and anisotropic displacement parameters. This material is available free of charge via the Internet at http://pubs.acs.org.

JA001886+

(33) Young, D. P.; Hall, D.; Torelli, M. E.; Fisk, Z.; Sarrao, J. L.; Thompson, J. D.; Ott, H.-R.; Oseroff, S. B.; Goodrich, R. G.; Zysler, R. *Nature* (London) **1999**, *397*, 412.

(34) Jarlborg, T. *Phys. Rev. Lett.* **2000**, *85*, 186.

(35) Certificate of analysis; Stock No. 42929; Lot no. K19J33; Alfa; Ward Hill, MA.